Precondensation phenomena in acoustic measurements

James B. Mehl[a] and Michael R. Moldover

Thermophysics Division, National Bureau of Standards, Washington, D.C. 20234
(Received 8 February 1982; accepted 12 March 1982)

Theoretical and experimental studies of the behavior of acoustic resonators whose walls are coated with a film of condensed vapor are reported. As a sound wave is reflected from the resonator walls, further condensation and evaporation will alter the thickness of the condensed film during the course of an acoustic cycle. We have modeled this effect for smooth walls and have calculated the associated specific acoustic admittance, which we refer to as β_{film}. Over a wide range of conditions, the magnitude of β_{film} is governed by the derivative of the film thickness with respect to pressure. Thus, for typical adsorption isotherms, the magnitude of β_{film} becomes large at very low pressures and at pressures just below the saturated vapor pressure. It seems possible that acoustic techiques could be used to study adsorption in both pressure regimes. If the resonator walls are rough (e.g., machined metal), a significant quantity of vapor will condense in the recesses of the walls at pressures well below the saturated vapor pressure. The specific acoustic admittance associated with such thick films is often more than ten times larger than the specific acoustic admittance predicted by the usual Kirchoff-Helmholtz formula. If this excess wall admittance is not recognized, the resonance frequencies will appear to imply an anomalous decrease in the speed of sound (c) as the saturated vapor pressure is approached. Such a decrease in the apparent value of c of nitrogen has been reported by Younglove and McCarthy, who observed decreases as large as 1%. We demonstrate that the same inhomogeneous precondensation phenomena can be easily be seen in propane at ambient temperature. These precondensation phenomena will influence measurements of acoustic virials at low temperatures, as well as the behavior of certain acoustic thermometers. Measurements of acoustic dissipative processes are also strongly affected. We have observed an increase of reflection losses by more than a factor of 200 as the pressure of propane on an aluminum surface was increased from 90% to 99.5% of the saturated vapor pressure.

I. INTRODUCTION

This study of precondensation phenomena in acoustic measurements was motivated by certain anomalous results encountered by Younglove and McCarty[1] in their recent measurements of the speed of sound in nitrogen gas. At low temperatures, as the two-phase boundary was approached, Younglove and McCarty observed a sharp decrease in the apparent speed of sound which "...appear(ed) to be in excess of what can be fitted with a virial equation..." (see Fig. 1).[1] In this article, we propose that this anomaly was an unrecognized consequence of the partial coating of the walls of the acoustic resonator used by Younglove and McCarty with a film of condensed nitrogen. We will also report our own new measurements of the speed of sound of propane as a function of pressure at 14.5 °C. As the pressure was raised above 90% of the saturated vapor pressure of propane, we also observed an anomalous decrease in the apparent speed of sound. This decrease could be as much as several percent, depending upon the experimental conditions. Because we made measurements with different resonators in the same gas at the same temperature and pressure, we are able to show experimentally, that at least in propane, the anomalous decrease in the apparent speed of sound is an artifact of the resonance technique. This artifact appears most strongly at low frequencies in resonators with large surface-to-volume ratios.

In an effort to understand the origin of this artifact, we have modeled the effects of multilayer adsorption on resonator performance. We considered a wall coated with a liquid film, and calculated the contribution to the specific acoustic admittance of the wall which is due to condensation and evaporation during the course of an acoustic cycle. The calculations can explain certain features of the Younglove–McCarty measurements on nitrogen and our own measurements on propane; however, a full theoretical understanding of the data will

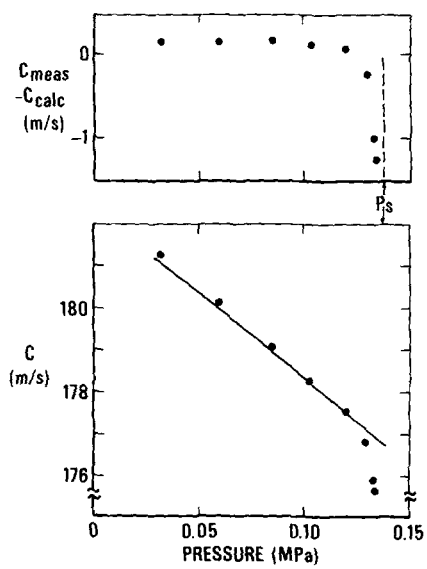

FIG. 1. Apparent speed of sound of nitrogen as a function of pressure at 80 K. (Top) Measured speed of sound (Ref. 1) less the speed of sound calculated as part of a correlation of the thermophysical properties of nitrogen (Ref. 4). (Bottom) The measurements of Ref. 1 are shown as points; the calculated values of Ref. 4 are shown as a smooth curve. The experimental data appear to show that the speed of sound decreases rapidly as P approaches P_s.

[a]Permanent address: Physics Department, University of Delaware, Newark, DE 19711.

probably require more detailed knowledge of the effects of the roughness of the interior surfaces of the resonators than we now have.

Our calculations of the film contribution to the specific acoustic admittance yielded the somewhat surprising result that the admittance of film-coated walls becomes large at very low pressures. The magnitude of the admittance is essentially determined by the pressure derivative of the film thickness, which we estimate from a theory of adsorption. Many standard adsorption isotherms have derivatives which become large or even diverge as the pressure approaches zero. To the best of our knowledge, the effects of adsorbed films at low pressures have not been observed in acoustics experiments.

The experiments and calculations we have carried out lead us to conclude that precondensation phenomena are an important limitation in using low-frequency (2–20 kHz) acoustic resonators (with both fixed and variable dimensions) to measure accurately ideal gas heat capacities and acoustic virial coefficients at low reduced temperatures with pressures very near the saturated vapor pressure. (Our calculations suggest that there may also be significant effects at much lower pressures.) These precondensation phenomena can be minimized by using resonators with "smooth" interior surfaces and low surface-to-volume ratios, and by making measurements with the higher frequency modes. The advantage of using higher frequencies is eventually defeated by the well-known limitations in the use of high frequency (> 1 MHz) acoustic resonators for measuring gas properties at low reduced temperatures, namely unacceptably large bulk losses and relaxation corrections, and unresolved modes.[2]

The remainder of this article is organized as follows. The experimental techniques and results are described in Sec. II and III. In Sec. IV we begin our theoretical discussion of precondensation phenomena in acoustic measurements by working out a model of the reflection of sound from a liquid film on a smooth boundary. The consequences of this model calculation are discussed in Sec. V. The model calculation is compared and contrasted with our experimental results in Sec. VI. There we propose that surface roughness plays a major role in the experiments.

II. EXPERIMENTAL TECHNIQUES

We begin with a brief review of the experiments of Younglove and McCarty.[1] The only details of their technique described here are those required for comparison with our own experiments, which are also described in this section.

Younglove and McCarty used a fixed path cylindrical invar resonator. Their resonator had an inner radius R of 5 mm, and a length L of 67 mm. The inside surface of their resonator was ground and polished. Both ends of their resonator were covered with aluminized polymer sheet transducers. These transducers were used to excite and detect longitudinal plane wave modes. The frequencies at which the detected amplitude passed through maxima (as observed on an oscilloscope) were measured with a frequency counter and recorded. In an idealized model, the frequencies of such longitudinal resonances would be given by

$$f_n = nc/(2L), \tag{1}$$

where c is the speed of sound in the gas and n is an integer identifying the mode. The data of Fig. 1 were taken using modes for which $n = 12$, 14, and 16.[3] The corresponding range of frequencies is 16–22 kHz. In order to obtain accurate values of the speed of sound from their measurements of resonance frequencies, Younglove and McCarty made the conventional corrections to their data. These corrections result from the viscous and thermal boundary layer effects at the resonator sides, and from the thermal boundary layer at the resonator ends. It is convenient to present the expressions for these corrections in a form which faciliates comparison with the anomalous precondensation effects which are under investigation in this work. The corrections can be expressed as

$$\Delta f + ig = [ic/(2\pi R)]\,[\beta_{\text{sides}} + (2R/L)\,\beta_{\text{ends}}]. \tag{2}$$

Here Δf is the frequency shift which must be added to the ideal resonance frequency f_n in order to obtain the experimental resonance frequency, and g is the resonance halfwidth (i.e., half the width of the resonance at $2^{-1/2}$ of maximum amplitude). The total specific acoustic admittance of a wall is defined as $\beta = \rho_g c u/p$, where u is the acoustic particle velocity in the gas normal to the wall, and p is the acoustic pressure in the gas. The boundary-layer contributions to the specific acoustic admittances of the sides and ends are given by

$$\beta_{\text{sides}} = (1+i)\,(\pi f/c)\,[(\gamma-1)\delta_{tg} + \delta_{vg}] \tag{3}$$

and

$$\beta_{\text{ends}} = (1+i)\,(\pi f/c)\,(\gamma-1)\,\delta_{tg}\,. \tag{4}$$

Here γ is the ratio of the specific heats C_p/C_v, δ_{tg} is the thermal penetration length in the gas, and δ_{vg} is the viscous penetration length in the gas. These lengths are given by

$$\delta_{tg} = [\lambda_g/(\rho_g C_{pg} \pi f)]^{1/2}\,, \tag{5}$$

and

$$\delta_{vg} = [\eta_g/(\rho_g \pi f)]^{1/2}\,, \tag{6}$$

where λ_g is the thermal conductivity, $\rho_g C_{pg}$ is the specific heat per unit volume, η_g is the viscosity, f is the frequency, and the subscript g denotes properties of the gas.

The magnitudes of the various terms in Eqs. (2)–(6) can be estimated from published thermophysical data. Relevant values are summarized in Table I for the conditions of the Younglove–McCarty experiments as well as for our own propane experiment. For nitrogen near 80 K and 1 MPa, the total fractional correction to the speed of sound given by Eq. (2) is approximately 0.1%.

Our measurements of the speed of sound in propane were made using three resonators. The first is an aluminum sphere (designated A) with an inside radius $a = 6.35$ cm, and a wall thickness of 1.27 cm. The sec-

TABLE I. Thermophysical properties and acoustic parameters of propane and nitrogen.

Quantity (unit)	Propane	Nitrogen	Nitrogen
T(K)	287.65	80	120
P_s(MPa)	0.720	0.137	2.51
c(m/s)	219	177	176
ρ_g(kg m^{-3})	15	6.1	125
ρ_l(kg m^{-3})	510	800	525
δ_{tg}(μm)[a]	4.5	6.0	1.1
δ_{tl}(μm)[a]	1.5	1.6	0.9
δ_{vg}(μm)[a]	4.1	5.4	1.6
δ_{vl}(μm)[a]	2.6	2.3	1.6
H(10^8 J m^{-3})	1.80	1.55	0.49
λ_g(mW m^{-1} K^{-1})	18	7.9	21
λ_l(mW m^{-1} K^{-1})	92	130	61
α_s(MPa K^{-1})	0.021 6	0.005 96	0.071 8
dP_s/dT(MPa K^{-1})	0.019 8	0.015	0.13
$\rho_l c\omega d_p[\ln(P_s/P)]^{4/3} \times P/P_s(10^{-6})$[a]	3.2	22	0.77
$\tau[\ln(P_s/P)]^{8/3}$(s)[b]	2.7×10^{-9}	2.9×10^{-7}	3.3×10^{-11}
ϕ	0.065	0.015	0.21
θ	0.019	0.16	0.08

[a]Values are for f = 10 kHz. [b]d_0 = 1 nm assumed.

ond is a brass sphere (designated B) with an inside radius of 3.17 cm and a wall thickness of 1.27 cm. The third is a brass cylinder (designated C) with a length L = 50 mm and an inside radius R = 5.2 mm. Thus resonator C has dimensions quite similar to those of the Younglove–McCarty resonator. All three resonators were mounted within the same pressure vessel and thermostat; thus the data from all three are taken with identical gas samples at identical temperatures and pressures. This thermostat has been thoroughly described elsewhere.[5]

Resonator A is essentially the same one described in Ref. 5. Several minor changes have been made to it in an effort to improve its suitability for making speed of sound measurements in gases at low pressures with an imprecision no greater than a few parts in one million.[6,7] In the present context, only one of the changes is likely to be significant: the interior surface was lightly polished with #600 abrasive paper. The interior surface of resonator B was not polished. Fine tooling marks are spaced at intervals of about 2.5 μm on resonator B. The machined finish of resonator C is much rougher; it was polished somewhat with abrasive but the surface is still coarse.

Aluminized polymer sheet transducers stretched over brass backing plates covered both ends of resonator C. These transducers are quite similar to the ones used by Younglove and McCarty. The transducers used to generate and detect sound in both spherical resonators are quite small and are installed in such a way as to minimize their influence upon the resonators's performance. The transducer used to generate sound in resonator A is 0.35 cm in diameter and is fitted into a snug hole so that is active surface is flush with the interior wall. This surface is a smooth aluminized polymer film backed by a flat brass electrode. Its acoustic admittance is not significantly different from that of the resonator walls. The detector transducer in resonator A is partially embedded in the resonator wall and coupled to the interior of the resonator by a hole, 0.08 cm in diameter and 0.64 cm long. Thus less than 0.001% of the interior surface of resonator A is perturbed by the transducers coupling hole. Both transducers used with resonator B were coupled to the interior through holes, 0.041 cm in diameter and 0.32 cm long. Thus only 0.002% of the walls of this resonator are perturbed by the transducer coupling holes.

The propane used in these measurements is stated to have a purity of 99.94% by the commercial supplier. We did not attempt further purification. The vapor pressure of our sample was 0.71993 MPa at 14.448 °C. This is 0.42% lower than the vapor pressure predicted by the equations of a recent correlation.[8] However, it is within the range of scatter of the data used to generate the equations of the correlation.

Only the radially symmetric modes of the spherical resonators were used in these measurements. In an idealized model, the frequencies of these resonances are given by an expression similar to Eq. (1)

$$f_p = c\,\mu_p/(2a)\ . \tag{7}$$

The first few eigenvalues μ_p in this equation are p = 1, 1.430 297; p = 2, 2.459 024; p = 3, 3.470 890; p = 4, 4.477 408; and p = 5, 5.481 537. The correction to the ideal resonance frequencies given by Eq. (7) is

$$\Delta f + ig = [ic/(2\pi a)]\,\beta_{\text{ends}} \tag{8}$$

with β_{ends} defined by Eq. (4). This correction arises from the thermal boundary layer at the inner wall of the sphere. Since the acoustic particle velocity is normal to this wall, there is no viscous boundary-layer correction for the radial modes. The radial modes are accordingly very sharp; at pressures well below the saturated vapor pressure the halfwidths g are on the order of 10^{-5} of the frequency f. A number of other minor corrections have been worked out in our previous work with the spherical resonator.[5–7] The propane measurements were all corrected for these effects.

At each pressure, we generally measured the frequency and width of the five lowest-frequency modes of resonator A, the three lowest-frequency modes of resonator B, and the longitudinal modes of resonator C with mode indices n = 1, 3, 5, 7, 9, and 11. For resonators A, B, and C these modes span the frequency range 2.5–10, 5–12, and 2–24 kHz, respectively. The data acquisition system and data processing procedures have been described elsewhere.[5] Here it is only important to note that the resonance frequencies and resonance halfwidth are both determined with a precision on the order of 0.1% of the resonance halfwidth g.

In order to determine the speed of sound from our measurements of the resonance frequencies of resonator C, we made the same corrections that Younglove and McCarty did [Eq. (2)]. Under the conditions of the propane experiments, the sums of the various fractional corrections to the resonance frequencies of the spheres were at least a factor of 10 smaller than the corresponding fractional corrections for the cylindrical resonator.

This results mainly from the absence of a viscous boundary layer with the radial modes of the spheres, and from the more favorable surface-to-volume ratio of the spheres.

Because spherical resonators are not widely used in acoustical studies of gases, we would like to make one remark. In previous work,[5] we have used resonator A to measure the speed of sound of ethylene at temperatures (0–100 °C), pressures (0.1–1 MPa), and frequencies (4–13 kHz) which overlap the present propane measurements. In that work it was shown that after the above-mentioned corrections were applied to the measured resonance frequencies, the apparent speed of sound, as determined using Eq. (7), for the first four radial modes, was independent of the mode at a level of 15 parts in 10^6. In the same work, our measured values of g/f agreed within ±10 parts in 10^6 of values calculated from independent, nonacoustic, data. Thus we have confidence, based on measurements, that the very much larger, mode dependent, discrepancies between the measured and predicted resonance frequencies (and between the measured and predicted resonance widths) which appear as the saturated vapor pressure of propane is approached are a consequence of the approach to saturation and not merely a consequence of inadequate modeling of spherical resonators.

III. EXPERIMENTAL RESULTS

Younglove and McCarty reported the results of detailed speed of sound measurements for nitrogen spanning temperatures from 80 to 350 K and pressures up to 1.5 MPa. Their data at 80, 90, 100, and 110 K include the region close to the two phase boundary. The speed of sound on each of these isotherms shows an anomalous decrease as the two-phase boundary is approached. The most marked decrease occurs at 80 K. In Fig. 1 we compare their data at 80 K with the speed of sound calculated from a complete correlation of the thermodynamic properties of nitrogen.[4] The correlation was not based on acoustic data, thus it should not be subject to systematic errors from the particular precondensation phenomena we are studying in this work.

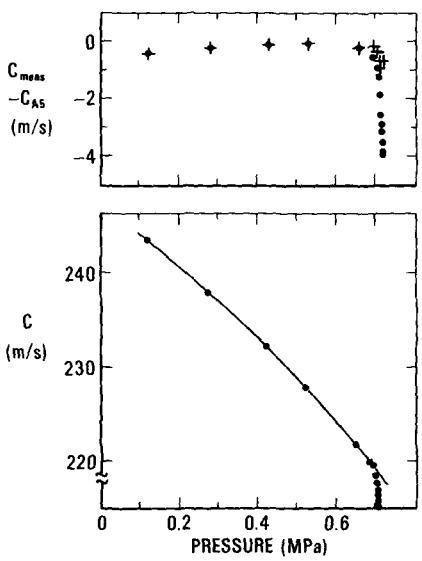

FIG. 2. Apparent speed of sound of propane as a function of pressure at 287.65 K. The measurements were made with the $n=1$ and $n=11$ modes of resonator C, and the $p=5$ mode of resonator A. (Top) Measurements taken with the C1 (solid circles) and C11 (crosses) modes, less measurements taken with the A5 mode. (Bottom) The smooth curve represents measurements taken with the A5 mode.

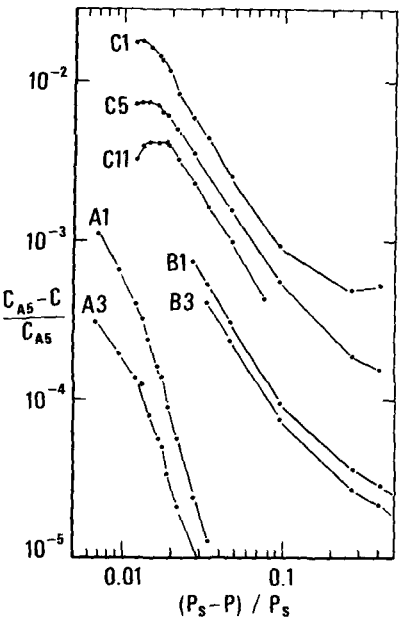

FIG. 3. Fractional deviations of the apparent measured speed of sound of propane c from a reference value c_{A5} as a function of the fractional deviation of the pressure P from the saturated vapor pressure P_s. The data were taken at 287.65 K with the $p=1$, 3, and 5 modes of resonator A, the $p=1$ and 3 modes of resonator B, and the $n=1$, 5, and 11 modes of resonator C. The lines connecting the points are intended only to guide the eye.

In Fig. 2 we present some of the speed of sound data for propane at 14.5 °C as a function of pressure. The solid curve represents the data taken with the $p=5$ mode of resonator A. (Over this range of pressures the lowest five radial modes yield values of c which agree within 0.04% of each other. This amount of dispersion is too small to be seen clearly even on the expanded scale in Fig. 2.) The solid points in Fig. 2 represent values of c determined with the $n=1$ mode of resonator C; the crosses represent data from the $n=11$ mode of resonator C. It is clear that if the data of resonator A are taken as a reference, the propane data taken with our cylindrical resonator show a precondensation anomaly which is very much like the anomaly that is shown for nitrogen in Fig. 1. It is also clear from Fig. 2 (and Fig. 3) that the anomaly becomes much stronger as the frequency is lowered. These qualitative features are present in our data from all three resonators. To exhibit this, we have chosen to use the apparent speed of sound as determined from the $p=5$ mode of resonator A as a reference. (It was not possible to use higher-frequency modes of resonator A, since those modes are significantly perturbed by the elastic resonances of the

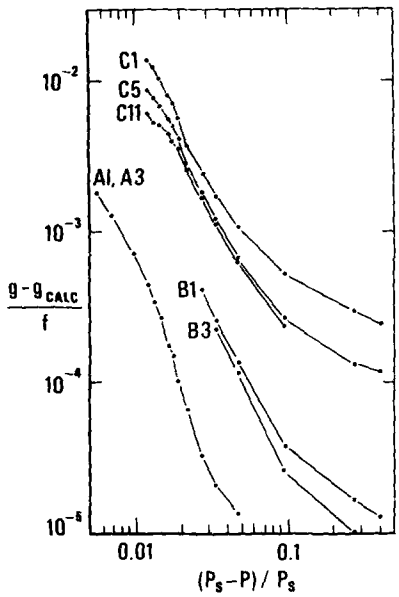

FIG. 4. The difference between the measured resonance halfwidth g and the calculated halfwidth g_{calc}, divided by the frequency f, as a function of the fractional deviation of the pressure P from the saturated vapor pressure P_s. The data were taken with propane at 287.65 K with the $p=1$ and 3 modes of resonator A, the $p=1$ and 3 modes of resonator B, and the $n=1$, 5, and 11 modes of resonator C. The lines connecting the points are intended only to guide the eye. The differences between the values of $(g-g_{calc})/f$ for the A1 and A3 modes are too small to be shown in the plot.

aluminum wall of the resonator.)

The apparent speed of sound, as determined with the $p=1$ and $p=3$ modes of resonators A and B, and the $n=1$, 5, and 11 modes of resonator C is shown as a function of pressure in Fig. 3. The ordinate is the reference speed of sound minus the apparent speed of sound for a particular mode, divided by the reference speed of sound. The abcissa is $(P_s-P)/P_s$, where P is the pressure and P_s is the saturated vapor pressure at the same temperature. Logarithmic scales conveniently spread out the data near P_s. The difference between the A1 and A3 measurements at a given pressure are an indication of the magnitude of the probable difference between the measurements taken with the A5 mode and the actual speed of sound. The data taken with resonators B and C show that the precondensation anomaly in the speed of sound is a resonator-dependent artifact which is most evident in the lower-frequency modes of a given resonator. In each case the data were taken up to the highest possible pressure. As P_s was approached, the signal amplitudes decreased more rapidly than we can account for on the basis of the increasing resonance halfwidths. Apparently the transducers become quite inefficient near P_s. Perhaps the space between the polymer sheet and its metal backing plate becomes filled with liquid propane.

The precondensation anomaly is also manifest in the excess resonance halfwidths observed as P approaches P_s. We expect contributions to the halfwidths from viscous and thermal boundary effects [Eqs. (2) and (8)] and from bulk dissipation. The latter contribution to g includes a classical contribution which depends upon the viscosity, thermal conductivity, and other parameters, and a relaxation contribution.[5] The contribution to g from classical bulk losses was included in all our calculations of g. This contribution was never more than a small fraction of the contribution from surface effects. Published data[9] indicate that the vibration-relaxation contribution for propane is negligible in this work.

In Fig. 4 we show the quantity $(g-g_{calc})/f$, which is the difference between the measured resonance halfwidths and the predicted halfwidths, divided by the measured frequency. All three resonators show an excess halfwidth which increases more than two orders of magnitude as P approaches P_s. The quantity $(g-g_{calc})/f$ decreases with increasing frequency for resonators B and C; it is fairly independent of frequency for resonator A. This is shown more clearly in Fig. 5, which shows data taken with as many as eleven radial modes with resonator A.

We have used Figs. 3 and 4 to emphasize that the precondensation anomaly is strongly dependent on the variable P_s-P. In Fig. 6 we compare the precondensation anomaly in the excess resonance widths with the precondensation anomaly in the apparent speed of sound (again using the $p=5$ mode of resonator A as a reference). The data are represented as an excess admittance of the boundary surface. For the cylindrical resonator (C) this is given by

$$i\beta=(2\pi R/c)[\Delta f+i\,(g-g_{calc})]/(1+2R/L), \tag{9}$$

and for the brass sphere (resonator B) by

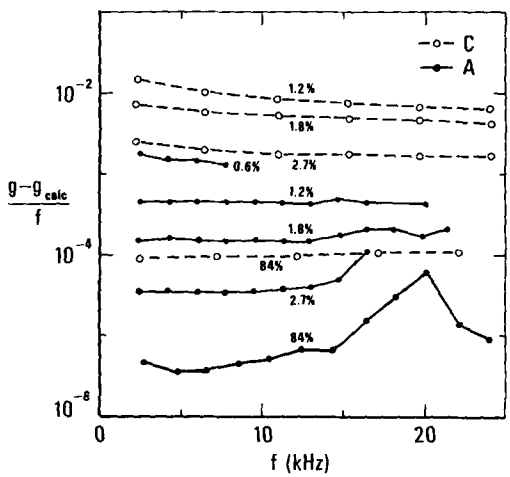

FIG. 5. The difference between the measured resonance halfwidth g and the calculated halfwidth g_{calc}, divided by the frequency f, as a function of f, for propane at 287.65 K and P near P_s. The lines connecting the points of a given data set are intended only to guide the eye. The data are labeled with the percentage deviation of the pressure P from the saturated vapor pressure P_s. The data were taken at 287.65 K with the $p=1$ to 12 modes of resonator A (solid symbols), and the $n=1$, 3, 5, 7, 9, and 11 modes of resonator C (open symbols). The lower pressure data taken with resonator A show the losses associated with the breathing resonance of the aluminum shell of the resonator at 20.2 kHz.

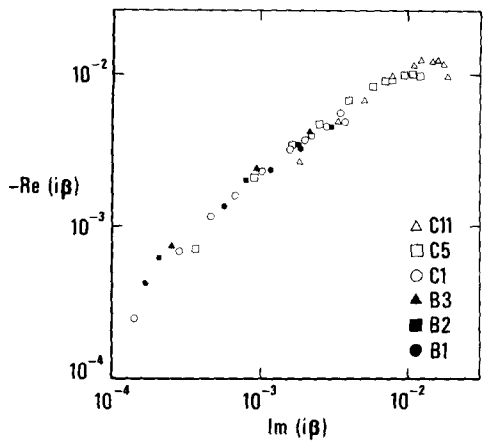

FIG. 6. The real and imaginary parts of the precondensation contribution to the specific acoustic admittance β of propane, for $T = 287.65$ K and P near P_s, plotted as $-\mathrm{Re}(i\beta)$ vs $\mathrm{Im}(i\beta)$. The quantity $-\mathrm{Re}(i\beta)$ is proportional to the frequency shift Δf; the quantity $\mathrm{Im}(i\beta)$ is proportional to $g - g_{\mathrm{calc}}$. The constants of proportionality for resonators B and C, as given in Eqs. (9) and (10) differ by a factor of 5. The fact that the two sets of data overlap in the figure is strong evidence for a surface effect.

$$i\beta = (2\pi a/c)[\Delta f + i(g - g_{\mathrm{calc}})] \ . \tag{10}$$

The ratio of the geometrical factors in Eqs. (9) and (10) is $R/[a(1+2R/L)] = 5.0$ The fact that the six sets of data in Fig. 6 overlap is strong experimental evidence for a surface effect, and furthermore, indicates a weak frequency dependence of the ratio: $-\mathrm{Re}(i\beta)/\mathrm{Im}(i\beta)$. The negative real part of $i\beta$, which is proportional to the anomaly in the apparent speed of sound tends to be about a factor of 2 higher than the imaginary part of $i\beta$, which is proportional to the excess halfwidth anomaly. This suggests that both anomalies could originate in a highly damped wave such as a thermal wave at the resonator walls. The observation is one of the motivations we have for considering, in the next section, an idealized model of the interaction between a sound wave and a wall covered with a film of condensed gas.

IV. ACOUSTIC ADMITTANCE OF A LIQUID FILM: A MODEL CALCULATION

In this section we estimate the very large enhancement of the specific acoustic admittance of a wall in contact with a condensible gas. We first consider a smooth plane wall that is coated with a film of condensed vapor of thickness d. The effect of surface roughness and the corresponding spatial variation of d is considered in Sec. VI. For the case of a smooth wall, we consider the effect of additional condensation and evaporation during the course of an acoustic cycle on the acoustic admittance of the wall. The extent of this additional condensation and evaporation will be limited by the rate at which the latent heat of condensation can be removed from the interface between the gas and the liquid film. Because material exchange occurs between the gas and the condensed layer, the acoustic particle velocity is not zero at this interface. When the gas density is low and when heat is rapidly conducted from the interface, the acoustic particle velocity will be much higher than that usually found at the interface between a noncondensible gas and a solid or a liquid.

The physical situation is sketched in Fig. 7. The wall is located in the half-space ($x < 0$). The condensed film in the interval ($0 \le x \le d$) is assumed to be sufficiently thick that its properties (density, thermal conductivity, specific heat, and latent heat of evaporation) are the same as those of the bulk liquid at the same temperature. The pressure gradient associated with the thermal wave[10] and with the acoustic wave in the gas ($d \ll c/f$) are quite small. Thus we take the acoustic pressure to be spatially uniform over the range of distances in Fig. 7.

Our physical model is based upon the application of several boundary conditions: at both the vapor–liquid and liquid–wall interfaces, we require conservation of mass, continuity of temperature, and continuity of heat flow.

We first consider the boundary conditions on the transverse components of the vapor and liquid velocities. The transverse particle velocity in the liquid near the wall must vanish. This can be satisfied in the usual way by introducing exponentially damped shear waves in the liquid and gas. These waves lead to a viscous contribution to the acoustic admittance of vapor–liquid interface of the form[11]

$$\beta_v = (1+i)\,(\pi f/c)(k_t/k)^2\,\delta_v \ . \tag{11}$$

Here k_t is the component of the wave vector of the acoustic wave in the vapor transverse to the wall, $k = \omega/c$ is the magnitude of the wave vector of the acoustic wave in the vapor, and δ_v is a suitable average of δ_{vg} and δ_{vl} which depends upon the film thickness d. [The viscous penetration length of the liquid δ_{vl} is defined by an equation similar to Eq. (6).] For ordinary fluids, $\delta_{vl} < \delta_{vg}$. Thus the viscous admittance of the film-covered wall is even less than that of the bare wall [the second term on the right-hand side of Eq. (3)] and thus is too small to require further consideration.

We next consider the boundary condition on the normal components of the vapor and liquid velocities. When the liquid–vapor system is somewhat below the critical point it is an excellent approximation to neglect the normal components of the acceleration of the liquid and the wall throughout the acoustic cycle. The boundary condition at the vapor–liquid interface is then

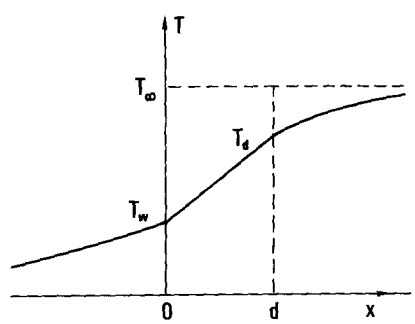

FIG. 7. Sketch of the amplitude of temperature oscillations near boundary surfaces which are coated with a liquid film. The interface between the metal wall and the liquid film is at $x = 0$; the interface between the liquid film and the vapor is at $x = d$.

$$u = u_{tg} - \dot{d}\rho_l/\rho_g \,, \tag{12}$$

where u_{tg} is the velocity associated with the thermal wave in the gas. The contribution of this term to the acoustic admittance will be on the order of β_{ends} [Eq. (4)]. Accordingly, it too is much smaller than the effects of interest here and will not be considered further. The remaining term in Eq. (12) is proportional to $\dot{d}$, the rate of change of the film's thickness resulting from condensation and evaporation in the course of an acoustic cycle. It is this term which leads to a major enhancement of both the real and imaginary parts of the acoustic admittance over the admittance arising from the viscous and thermal boundary layers.

We next consider the balance of heat flow at the vapor–liquid interface. The condensing gas deposits its latent heat at $x = d$. This acts as a heat source whose strength (per unit area) is

$$S = H\dot{d} \,, \tag{13}$$

where H is the latent heat per unit volume of liquid. The rate of condensation will be limited by the rate at which heat is conducted away from the interface; we thus consider the temperature distribution sketched in Fig. (7). We assume an implicit time dependence proportional to $e^{i\omega t}$. For notational convenience we introduce the symbols k_w, k_l, and k_g for the complex propagation constants of thermal waves in the wall, liquid, and gas, respectively. These are related to the corresponding thermal penetration lengths by equations of the form

$$k_w = (1+i)/\delta_{tw} \,, \tag{14}$$

where δ_{tw} and δ_{tl} are defined by equations similar to Eq. (5). The following equations describe the spatial dependence of the temperature waves

$$\begin{aligned} T(x) &= T_w e^{k_w x} && \text{(wall)}, \\ &= T_1 e^{k_l x} + T_2 e^{-k_l x} && \text{(liquid)}, \\ &= T_\infty - T_3 e^{-k_g x} && \text{(vapor)}. \end{aligned} \tag{15}$$

Here T_∞, the amplitude of the temperature oscillations associated with the acoustic wave far from the wall, is related to the acoustic pressure through

$$p = (\partial P/\partial T)_s T_\infty \equiv \alpha_s T_\infty \,. \tag{16}$$

Continuity of the temperature at $x = 0$ and $x = d$ requires

$$T_w = T_1 + T_2$$

and

$$T_1 e^{k_l d} + T_2 e^{-k_l d} = T_\infty - T_3 e^{-k_g d} \,. \tag{17}$$

The heat flux at $x = 0$ must be continuous:

$$\lambda_w k_w T_w = \lambda_l k_l (T_1 - T_2). \tag{18}$$

The discontinuity in the heat flux at $x = d$ must equal the heat source there [Eq. (13)]:

$$S = -\lambda_g k_g T_g e^{-k_g d} + \lambda_l k_l (T_1 e^{k_l d} + T_2^{-k_l d}). \tag{19}$$

Our last assumption is that the film is always in local thermodynamic equilibrium. Then the rate of change of the film thickness is related to the time dependence of the temperature and pressure at the liquid–vapor interface through

$$\dot{d} = i\omega d_P p + i\omega d_T (T_1 e^{k_l d} + T_2 e^{-k_l d}), \tag{20}$$

where $d_P = (\partial d/\partial P)_T$ and $d_T = (\partial d/\partial T)_P$. The specific acoustic admittance at the film surface, $\rho_g c u/p$, is obtained by combining Eqs. (12), (13), and (15)–(20). The result is

$$i\beta_{\text{film}} = -\rho_l c \omega d_P \frac{1 + [1 + d_T/(\alpha_s d_P)]\,\phi \tanh(\theta + k_l d)}{1 + [1 - (1+i)\sqrt{\omega\tau}]\,\phi \tanh(\theta + k_l d)} \,, \tag{21}$$

where θ, ϕ, and τ are defined by

$$\begin{aligned} \theta &= \tanh^{-1}[\lambda_l k_l/(\lambda_w k_w)], \\ \phi &= \lambda_g k_g/(\lambda_l k_l), \end{aligned} \tag{22}$$

and

$$\tau = (H d_T)^2/(2\lambda_g C_{pg} \rho_g).$$

In order to evaluate Eq. (21) we require the "equation of state" of the film $d(P, T)$. We shall use the theory of Dzyaloshinskii *et al.*[12] for this purpose. When the dominant interaction between the fluid and the wall is the London–van der Waals force, the thickness of the film can be expressed in terms of a characteristic frequency $\bar{\omega}$ through[12]

$$\ln(P/P_s) = (\hbar\bar{\omega}m)/(8\pi^2 d^3 \rho_l k_B T). \tag{23}$$

Here $\hbar$ is Planck's constant, k_B is Boltzmann's constant, and m is the mass of a propane molecule. The characteristic frequency $\bar{\omega}$ is related to the electronic polarizability of the fluid and wall. It can be obtained from the frequency-dependent complex dielectric constants of the metal substrate and the liquid propane adsorbate through[12]

$$\bar{\omega} = \int_0^{i\infty} \frac{(\epsilon_l - 1)(\epsilon_l - \epsilon_w)}{(\epsilon_l + 1)(\epsilon_l + \epsilon_w)}\, d(i\omega) \,. \tag{24}$$

In many cases $\bar{\omega}$ may be evaluated with an accuracy on the order of 10% by using spectroscopic information. For our purposes, a very crude approximation will suffice. We make the rough approximation that $\epsilon_w \gg \epsilon_l$ at all frequencies of interest. We approximate ϵ_l with the dielectric function of an oscillator whose static dielectric response corresponds with that of liquid propane at 15 °C ($\epsilon = 1.6$), and whose resonance frequency is equal to the ionization potential of propane divided by Planck's constant. Above this resonance frequency, we interpolate to the dielectric response of a plasma as suggested by Ninham and Parsegian.[13] These approximations yield $\bar{\omega} \approx -2\times10^{16}$ Hz. When this is used in Eq. (24) we obtain

$$d = d_0[\ln(P_s/P)]^{-1/3} \,, \tag{25}$$

with the constant d_0 equal to approximately 1 nm. We have used this as our "equation of state" of the film in order to estimate the acoustic admittance predicted by Eq. (21).

We expect Eq. (25) to be reasonably accurate for values of d greater than a few atomic diameters but smaller than the ratio of the speed of light to $\bar{\omega}$ (15 nm). This range of expected validity corresponds to $10^{-3} < P/P_s < 0.9995$. For values of d greater than about 15 nm, retardation effects[12] will gradually change the exponent in Eq. (25) from $-1/3$ to $-1/4$. For values of less d

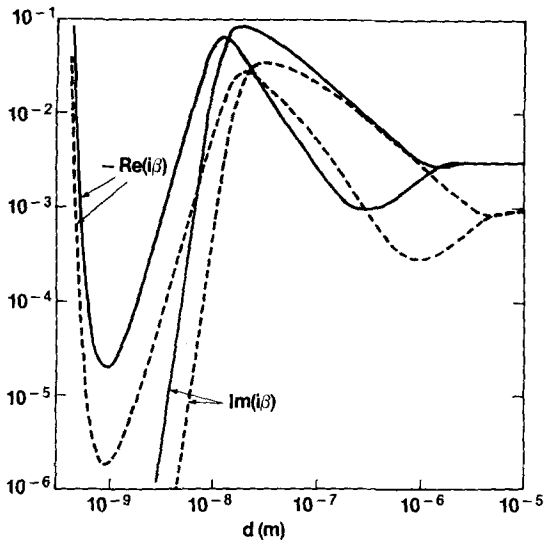

FIG. 8. The precondensation contribution to the specific acoustic admittance β of propane at 287.65 K and P near P_s, calculated with Eq. (21) as a function of the film thickness d. The solid lines are for $f = 24$ kHz, the approximate frequency of the C11 mode, and the dashed lines are for $f = 2.2$ kHz, the approximate frequency of the C1 mode. The parameters of Table I and the equation of state of the film [Eq. (25)] were used in the calculation.

than a few molecular diameters the theory of Dzyaloshinskii *et al.* is not applicable.

The temperature and pressure derivatives of d are needed for the evaluation of Eq. (21). The temperature dependence of d_0 given by Eq. (23) and implicit in Eq. (24) does not contribute significantly to d_T. The main contribution comes from the slope of the saturated vapor pressure curve. Differentiating Eq. (25), we thus obtain $d_T \approx -d_P(P/P_s)dP_s/dT$, where d_P can be calculated directly from Eq. (25). Numerical values of the parameters in Eq. (25) obtained in this way are given in Table I. Results of the calculation of the specific acoustic admittance are shown in Fig. 8, for frequencies of 2.2 and 24 kHz, which equal the frequencies of the $n = 1$ and $n = 11$ modes of resonator C, and also bound the range of experimental frequencies. The calculated curves are compared with our propane measurements of the real and imaginary parts of the specific acoustic admittance in Fig. 9.

V. DISCUSSION OF THE ADMITTANCE ENHANCEMENT

The specific acoustic admittance β_{fillm} shown in Fig. 8 has a complicated structure. The significant features can be understood by considering the predictions of Eq. (21) in some limiting cases.

For thick films Eq. (21) reduces to

$$i\beta_{\mathrm{fillm}} = (-1+i)(c\lambda_l\rho_l)/[H\delta_{sl}(dP_s/dT)] \quad . \tag{26}$$

This expression is independent of the film thickness; thus it also applies to the reflection of sound at an interface between the vapor and bulk liquid. Equation (26) has real and imaginary parts of the same magnitude. The boundary-layer correction of Kirchoff and Helmholtz [Eq. (3)] has this same property. Since the viscous boundary layer normally dominates in Eq. (3), a useful comparison is the ratio of Eq. (26) to the viscous part of Eq. (3)

$$\beta_{\mathrm{fillm}}/\beta_{\mathrm{viscous}} = [c^2\rho_l/(H\,dP_s/dT)][\rho_g\rho_l\lambda_l c_{pl}/\eta_g]^{1/2} \quad . \tag{27}$$

Under the conditions of our propane experiment, the ratio given by Eq. (27) is approximately 10; for the Younglove–McCarty measurement in nitrogen, the ratio is 5.2 at 80 K and it declines at higher temperatures. [None of the results in this article should be used very near the critical point, where Eq. (27) diverges.] We conclude that thick films can enhance the frequency shifts and losses which originate along the walls of a cylindrical resonator by a factor on the order of 5 to 10. Because the conventional contributions to the admittance for the radial modes of a spherical resonator are much smaller than β_{viscous}, the ratio of film effects to conventional effects would be correspondingly greater.

The expression for β_{fillm} in the very thick film limit [Eq. (26)] appears to diverge at low temperatures where dP_s/dT approaches zero. Several phenomena which we have neglected suppress this apparent divergence. We have assumed that local thermodynamic equilibrium is always valid and that the mean free path in the gas is zero (or, equivalently, that a hydrodynamic description is valid). Robnik *et al.*[14] considered the reflection of sound from a liquid under low pressure conditions where these assumptions begin to fail ($P_s \approx 0.001$ MPa). They calculate a finite acoustic admittance which is related to the phenomenological jump coefficients which appear in kinetic theory.

We next consider thin films, with d in the range from 5×10^{-10} (one molecular layer) to 10^{-8} m. This upper

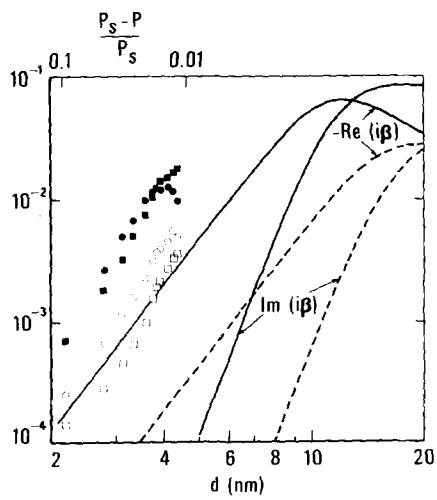

FIG. 9. The precondensation contribution to the specific acoustic admittance β of propane at 287.65 K and P near P_s. The solid and dashed lines are identical with those in Fig. 8 over a truncated range of film thickness d. The symbols represent values of $-\mathrm{Re}(i\beta)$ (circles) and $\mathrm{Im}(i\beta)$ (squares), calculated from measurements taken with the $n = 1$ (open symbols) and $n = 11$ (solid symbols) modes of resonator C, using Eq. (9). A relative pressure scale is indicated at the top of the figure.

bound is determined by the condition $|k_l d| < \theta$. In this range, a reasonable approximation to Eq. (21) is given by

$$i\beta_{fllm} = -\rho_l c\,\omega d_P \{1 + (1+i)Hd_T[\omega/(2\lambda_w \rho_w c_{pw})]^{1/2}\}, \tag{28}$$

with d_P and d_T given by

$$d_P(3P_s/d_0) = (P_s/P)[\ln(P_s/P)]^{-4/3} = (d/d_0)^4 e^{(d_0/d)^3} \tag{29}$$

and

$$d_T(3P_s/d_0) = [\ln(P_s/P)]^{-4/3} = (d/d_0)^4 . \tag{30}$$

In this range the thickness (or pressure) dependence of β_{fllm} is completely dominated by the behavior of d_P displayed in Eq. (29). Thus the very sharp minimum in $-\mathrm{Re}(i\beta_{fllm})$ which occurs near $d = d_0$ (or $P = 0.3P_s$) is simply a reflection of the pronounced minimum which occurs in the pressure derivative of the adsorption isotherm Eq. (25). In this range of thicknesses the acoustic losses, which are proportional to $\mathrm{Im}(i\beta_{fllm})$, depend upon the thermal conductivity of the wall, but not on the thermal conductivity of the liquid. The films are so thin that the amplitude of the thermal wave in the liquid [(Eq. (15)] is nearly constant. For very thin films, the assumption that d_T can be obtained directly from Eq. (25) eventually fails to be reasonable. Since the acoustic losses in this range are proportional to d_T, it is difficult to predict these losses for very thin films. [To avoid confusion in Fig. 8 we have not plotted $\mathrm{Im}(i\beta_{fllm})$ for $d < 1$ nm. Note that Eq. (28) predicts a divergence of this quantity as d becomes small.]

For the intermediate range of thicknesses ($10^{-8}\,\mathrm{m} < d < 5\times10^{-6}\,\mathrm{m}$) the full expression Eq. (21) is required for calculation of β_{fllm}. The broad minima in $-\mathrm{Re}(i\beta_{fllm})$ which occur near $d = 3\times10^{-7}\,\mathrm{m}$ are associated with the growth of the term $\sqrt{\omega\tau}$ in the denominator of Eq. (21). This term becomes much larger than unity as P approaches P_s as a consequence of the divergence of $\sqrt{\tau}$, which is proportional to d_T. In this range of d we would expect Eq. (25) to require modification for the effects of of retardation; however, the qualitative shape of the curves in Fig. 8 would not be significantly affected by this change.

VI. COMPARISON OF EXPERIMENT AND THEORY

Figure 9 shows some of our experimental values of $i\beta_{fllm}$, the specific acoustic admittance of propane. The measurements were made with the cylindrical resonator. Equation (9) was used to determine $i\beta_{fllm}$ from our measurements of the shift in the resonance frequencies and the excess resonance halfwidths. Plots of the admittance calculated from Eqs. (21) and (25) are shown for comparison. The data are plotted as a function of pressure (note the scale at the upper left) while the calculated curve is plotted as a function of the film thickness d. Equation (25) was used to relate pressure to film thickness. This relation is based on the assumption that the resonator walls are smooth.

It is clear that the data plotted in Fig. 9 have many qualitative features which are in agreement with our theory. Among these are: (1) As the film thickness and pressure decrease, both $-\mathrm{Re}(i\beta_{fllm})$ and $\mathrm{Im}(i\beta_{fllm})$ decrease rapidly. (2) The measured admittance is higher at low frequencies. (3) As the film thickness and pressure increase, $-\mathrm{Re}(i\beta_{fllm})$ reaches a maximum. This maximum is more pronounced and occurs at lower pressures for the higher-frequency data (C11). The same trend was evident in data from four modes (C3, C5, C7, and C9) which are not shown in Fig. 9. The maximum increases with frequency. (4) In the same range of pressures, we observed no maxima in $\mathrm{Im}(i\beta_{fllm})$. This is consistent with the calculated curves, which show that the maxima in $\mathrm{Im}(i\beta_{fllm})$ occur at higher film thicknesses than the maxima in $-\mathrm{Re}(i\beta_{fllm})$ at all frequencies.

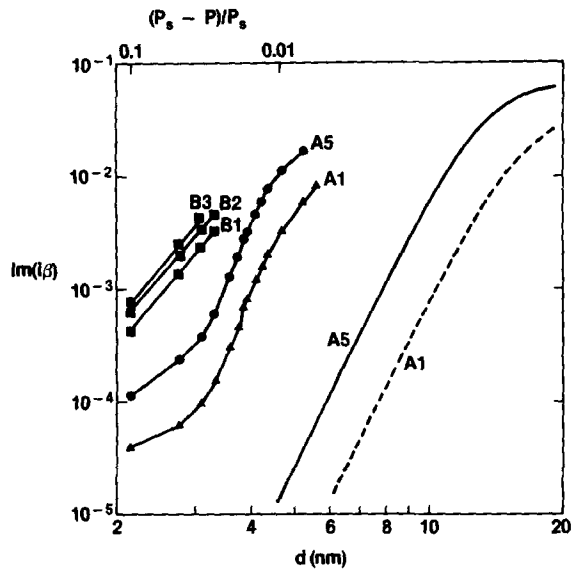

FIG. 10. The precondensation contribution to the imaginary part of the specific acoustic admittance of propane at 287.65 K and P near P_s. The solid curves were calculated with Eqs. (21) and (25) using the frequencies of 2.5 and 9.5 kHz, corresponding to the $p = 1$ and 5 modes of resonator A. The symbols represent values of $\mathrm{Im}(i\beta)$ calculated from measurements taken with the $p = 1$ and 5 modes of the resonator A, and the $p = 1$, 2, and 3 modes of resonator B, using Eq. (10). A relative pressure scale is indicated at the top of the figure.

Figure 6 shows that measurements of β_{fllm} made with the brass spherical resonator B and the brass cylindrical resonator C are in close agreement. Since the $p = 5$ mode of the aluminum spherical resonator A was used as a reference in determination of $-\mathrm{Re}(i\beta_{fllm})$, we have no reliable estimates of this quantity for resonator A. Measurements of $\mathrm{Im}(i\beta_{fllm})$ with resonators A and B are shown in Fig. 10. The data from resonator A are consistently lower by a factor of about 5, and lie closer to the theoretical curves. The slopes of the data taken with resonator A also appear to be in closer agreement with the theoretical curves. The measurements taken with resonator A extend to slightly higher pressures than those taken with resonator C. The trend toward a peak is evident in the higher pressure data, in agreement with the theoretical curves.

Plots of the data of Younglove and McCarty[1] at 90,

100, and 120 K are qualitatively similar to the plot of the 80 K data in Fig. 1, except that the magnitude of the anomaly in the apparent speed of sound decreases with increasing temperature. Calculated values of $-\mathrm{Re}\,(i\beta_{film})$, which is proportional to the apparent shift in the speed of sound, show a general decrease, including a decrease of the maximum, with increasing temperature. Thus our calculations are in qualitative agreement with the measurement of Younglove and McCarty in nitrogen. The parameters in Eq. (21) applicable to the nitrogen experiment of Younglove and McCarty are listed in Table I. Note that the magnitude of the prefactor $-\rho_l \omega c d_P$ in Eq. (21) lies in the same general range for propane and nitrogen over a range of temperatures considered.

The most important qualitative difference between the data and calculated curves in Figs. 9 and 10 is that the measured values of $-\mathrm{Re}\,(i\beta_{film})$ and $\mathrm{Im}\,(i\beta_{film})$ greatly exceed the calculated values at the same pressure. Also, the maximum measured values are about one order of magnitude lower than the theoretical maxima. The measured frequency dependence of $\mathrm{Im}\,(i\beta_{film})$ also appears to be in disagree with the theory: Fig. 5 shows that the acoustic losses, which are proportional to $g - g_{calc}$ and hence to $\mathrm{Im}\,(i\beta_{film})$, are proportional to the frequency f over a wide range of conditions, particularly for resonator A. The same trend was observed with resonator B. The theoretical curves show a different frequency dependence: in the thin film region, $\mathrm{Im}\,(i\beta_{film})$ is approximately proportional to $f^{3/2}$, as can be seen from Eq. (28). We believe these differences are qualitatively consistent with the expected effects of wall roughness.

Equation (25), which predicts the thickness of the precondensed film, is based on the assumption of a smooth wall. The London–van der Waals interaction has been calculated for geometries other than the infinite half-space assumed in Eq. (24)[15]; however, none of these geometries can be considered as reasonable models for a rough metal surface. One would expect, however, that a calculation for a realistic geometry would yield results consistent with the phenomenological Young–LaPlace equation

$$P_s - P = 2\sigma/r \ . \tag{31}$$

Thus we expect concave portions of a rough surface to be completely filled with liquid until the local average radius of curvature r is consistent with Eq. (31). Using 0.01 N/m as an estimate of the surface tension σ in Eq. (31), we estimate that the tooling marks on the walls of resonator B (which have a characteristic size on the order of 10^{-6} m) will be completely filled with liquid at $(P_s - P)/P_s = 0.03$, which is near the center of the significant range of pressure in our experiment. Thus it is likely that the film coating the walls of this resonator is quite inhomogeneous. On concave portions of the wall the film thickness d will be on the order of 10^{-6} m while on convex portions of the wall d will be on the order of 3×10^{-9} m. Under such conditions, measurements of the admittance will be averages over a substantial range of d. In such an average, the portions of the wall for which $i\beta_{film}$ has maximum magnitude will be most influential. The frequency dependence of $i\beta_{film}$ is different in the different ranges of d (see Fig. 8). For example, in the thin film region $\mathrm{Im}\,(i\beta_{film})$ is proportional to $f^{3/2}$ and $-\mathrm{Re}\,(i\beta_{film})$ is proportional to f, while the maxima of both quantities are approximately proportional to $f^{1/3}$. Thus it is difficult to predict the frequency dependence of the spatial average of $i\beta_{film}$, other than to note the general trend towards an increase in frequency. Our measurements show that $\mathrm{Im}\,(i\beta_{film})$ tends to be proportional to the frequency over the full range of frequencies of the experiment (see Fig. 5). We have not observed as consistent a trend in the frequency dependence of $-\mathrm{Re}\,(i\beta_{film})$, but this quantity is approximately proportional to a low power of the frequency, similar to the frequency dependence of the maximum theoretical value. We conclude that our observed frequency dependence of β_{film} is qualitatively consistent with our theory.

Our observation of frequency-dependent peaks in $-\mathrm{Re}\,(i\beta_{film})$ which are lower than the predicted peaks is also consistent with an inhomogeneous film picture. The thickness corresponding to the peak of $-\mathrm{Re}\,(i\beta_{film})$ will occur in different portions of the surface as the pressure is varied. At any given pressure, the average of $-\mathrm{Re}\,(i\beta_{film})$ will be less than the peak value, in agreement with our measurements.

We have also made some preliminary measurements at pressures below those shown in the figures. In some of these measurements there is an indication of the increase in $-\mathrm{Re}\,(i\beta_{film})$ which is expected at low pressures. This effect is a subject for further investigation.

VII. CONCLUDING REMARKS

We have demonstrated that the apparent decrease in the speed of sound as the pressure is increased toward the saturated vapor pressure P_s is an experimental artifact, which is most pronounced at low frequencies and in resonators with rough walls and large surface to volume ratios.

Our theoretical model of precondensation effects correctly predicts several qualitative features of the experimental results. The model also predicts a similar "artifact" in speed of sound measurements at pressures below about $0.3P_s$, when the adsorbed film is only a few molecular diameters thick. This low pressure anomaly should be explored with care: it may have important consequences in those applications (such as acoustic thermometry) which require low-frequency speed of sound measurements of the highest possible accuracy. At low pressures, the predicted value of $-\mathrm{Re}\,(i\beta_{film})$ is proportional to the frequency [Eq. (28)]; thus measurements of the speed of sound with several resonances of a single, fixed geometry, resonator cannot detect the predicted precondensation effect. The different resonances will yield internally consistent values of the speed of sound which are systematically too low, and which become even lower as the temperature is reduced. Measurements of the resonator losses can reveal the presence of this precondensation effect as an anomalous excess loss. However, the predicted values of $-\mathrm{Re}\,(i\beta_{film})$ greatly exceed the values of

Im ($i\beta_{film}$) at low pressures; thus such excess losses cannot fully reveal the extent of the systematic errors. Only measurements in which the same gas is studied in one or more resonators with different surface-to-volume ratios can reveal such errors. In this work we used three fixed geometry resonators to vary the surface-to-volume ratio.

Up to this point we have discussed resonators with a fixed geometry. We now note that certain low-frequency variable path acoustic interferometers[2] are also subject to systematic errors if precondensation phenomena are not recognized. These interferometers are often excited by a source of fixed frequency built into one end of a cylindrical resonator. The amplitude and/or phase of the standing wave in the resonator is measured as a function of the displacement of the other end of the resonator. In effect, both n and L in Eq. (1) are varied simultaneously. The apparent speed of sound obtained from such data is essentially independent of the admittance of the resonator ends even when there is a precondensed film on them. However, any precondensation contribution to the admittance of the resonator sides will influence the apparent speed of sound. To first approximation, β_{sides} in Eq. (2) must be replaced by $\beta_{sides}+\beta_{film}$. It follows that these variable path interferometers are subject to the same systematic errors as the fixed path resonators which we have discussed above.

ACKNOWLEDGMENTS

The authors are grateful to Ben A. Younglove and R. D. McCarty for providing unpublished details of their work. One of us (MRM) is grateful to V. A. Parsegian for some helpful comments about dispersion forces.

[1]Ben A. Younglove and Robert D. McCarty, J. Chem. Thermodyn. 12, 1121 (1980).
[2]A. R. Colclough, Metrologia 9, 75 (1973).
[3]Ben A. Younglove (private communication).
[4]R. T. Jacobsen, R. B. Stewart, R. D. McCarty, and H. J. M. Hanley, Natl. Bur. Stand. (U.S.) Tech. Note 648 (1973).
[5]J. B. Mehl and M. R. Moldover, J. Chem. Phys. 74, 4062 (1981).
[6]M. R. Moldover and J. B. Mehl, in *Proceedings of the Second International Conference on Precision Measurements and Fundamental Constants*, 1981 (National Bureau of Standards, Washington, D.C., to be published).
[7]J. B. Mehl and M. R. Moldover, in *Proceedings of the Eighth Symposium on Thermophysical Properties*, 1981 (National Bureau of Standards, Washington, D.C., to be published).
[8]R. D. Goodwin, "Provisional Thermodynamic Functions of Propane, from 85 to 700 K at Pressures to 700 bar," NBSIR 77–860 (National Bureau of Standards, Washington, D.C., 1977).
[9]R. Holmes, G. R. Jones, and N. Pusat, J. Chem. Phys. 41, 2512 (1961).
[10]P. M. Morse and K. U. Ingard, *Theoretical Acoustics* (McGraw–Hill, New York, 1969), pp. 281–291.
[11]Reference 10, Eq. (6.4.36).
[12]I. E. Dzyaloshinskii, E. M. Lifshitz, and L. P. Pitaevskii, Adv. Phys. 10, 165 (1961).
[13]B. W. Ninham and V. A. Parsegian, J. Chem. Phys. 52, 4578 (1970).
[14]Marko Robnik, Ivan Kuscer, and Heinz Lang, Int. J. Heat Mass Transfer 22, 461 (1979).
[15]See e.g., J. Mahanty and B. W. Ninham, *Disperson Forces* (Academic, New York, 1976), Chap. 5.